AMERICAN SOCIETY FOR MICROBIOLOGY | Molecular and Cellular Biology®

RESEARCH ARTICLE

USP15 Deubiquitinates TUT1 Associated with RNA Metabolism and Maintains Cerebellar Homeostasis

Jaehyun Kim,[b] Junnosuke Nakamura,[b] Chiharu Hamada,[b] Takumi Taketomi,[c] Sarasa Yano,[b] Tomomi Okajima,[b] Shin-ichi Kashiwabara,[a,d] Tadashi Baba,[a,d] Ban Sato,[a] Tomoki Chiba,[a,d] Fuminori Tsuruta[a,d,e]

[a]Faculty of Life and Environmental Sciences, University of Tsukuba, Tsukuba, Ibaraki, Japan
[b]Graduate School of Life and Environmental Sciences, University of Tsukuba, Tsukuba, Ibaraki, Japan
[c]College of Biological Sciences, School of Life and Environmental Sciences, University of Tsukuba, Tsukuba, Ibaraki, Japan
[d]Ph.D. Program in Human Biology, School of Integrative and Global Majors, University of Tsukuba, Tsukuba, Ibaraki, Japan
[e]Master's and Doctoral Program in Neuroscience, Graduate School of Comprehensive Human Sciences, University of Tsukuba, Tsukuba, Ibaraki, Japan

Junnosuke Nakamura, Chiharu Hamada, and Takumi Taketomi contributed equally to this work.

ABSTRACT Precise regulation of RNA metabolism is crucial for dynamic gene expression and controlling cellular functions. In the nervous system, defects in RNA metabolism are implicated in the disturbance of brain homeostasis and development. Here, we report that deubiquitinating enzyme, ubiquitin specific peptidase 15 (USP15), deubiquitinates terminal uridylyl transferase 1 (TUT1) and changes global RNA metabolism. We found that the expression of USP15 redistributes TUT1 from the nucleolus to nucleoplasm, resulting in the stabilization of U6 snRNA. We also found that lack of the *Usp15* gene induces an impairment in motor ability with an unconventional cerebellar formation. Moreover, inhibition of the USP15-TUT1 cascade triggered mild and chronic endoplasmic reticulum (ER) stress. Therefore, our results suggest that USP15 is crucial for mRNA metabolism and maintains a healthy brain. These findings provide a possibility that disturbance of the USP15-TUT1 cascade induces chronic and mild ER stress, leading to an acceleration of the neurodegenerative phenotype.

KEYWORDS ER stress, RNA metabolism, TUT1, USP15, cerebellum

RNA metabolism depicts the entire events that occurred in the life cycle of RNA from its synthesis and modification to degradation, leading to the control of protein diversity. Alternative mRNA splicing is one of the pivotal processes that underlie global RNA metabolism. This machinery is essential for protein diversity, which enables eukaryotic cells to produce various proteins with different functions at a specific stage from a single gene (1). In the nervous system, the regulation of mRNA metabolism plays an important role in a variety of events such as development, synaptogenesis, the sculpting of neuronal circuits, and survival (2, 3). Mutations in genes associated with RNA metabolism have been implicated in developmental defects and several neurodegenerative disorders such as amyotrophic lateral sclerosis and Parkinson's disease (4). Therefore, a deteriorating RNA metabolism tightly associates with disturbed brain homeostasis.

Alternative splicing involves the macromolecular complex known as the spliceosome, which consists of five small nuclear ribonucleoproteins (snRNPs) and multiple snRNP-related proteins (5). It is initiated by the binding of U1 snRNP to the 5′ splice site and the recognition of U2 snRNP to the branching point located upstream of the 3′ splice site. U4/U6.U5 tri-snRNPs are recruited subsequently to establish the spliceosome, and U1 and U4 snRNPs are disassembled for catalytical activation of the spliceosome by conformational rearrangement. The activated spliceosome splices and

Citation Kim J, Nakamura J, Hamada C, Taketomi T, Yano S, Okajima T, Kashiwabara S-I, Baba T, Sato B, Chiba T, Tsuruta F. 2020. USP15 deubiquitinates TUT1 associated with RNA metabolism and maintains cerebellar homeostasis. Mol Cell Biol 40:e00098-20. https://doi.org/10.1128/MCB.00098-20.

Address correspondence to Tomoki Chiba, tchiba@biol.tsukuba.ac.jp, or Fuminori Tsuruta, tsuruta.fuminori.fn@u.tsukuba.ac.jp.

Received 11 March 2020
Returned for modification 13 April 2020
Accepted 13 August 2020
Accepted manuscript posted online 24 August 2020
Published 13 October 2020

releases introns and ligates exons by terminating the splicing reaction. Genetic disruptions in this process impair normal mRNA turnover and increase the risk of aberrant brain development and neurodegenerative disorders, indicating that these processes are essential for healthy brain homeostasis. Recently, the ubiquitin and ubiquitin-like proteins have emerged as key machinery for mRNA turnover. Comprehensive proteomics has revealed that ubiquitin and ubiquitin-like proteins are incorporated into the spliceosome (6, 7). A ubiquitin mutant that attenuates the binding affinity toward ubiquitin-interacting motif abolishes the assembly and disassembly of U4/U6.U5 tri-snRNPs (8). A deubiquitinating reaction controls the rearrangement of U4/U6.U5 tri-snRNPs, leading to changes in splicing patterns (9, 10). These studies demonstrate that the ubiquitin systems are essential for mRNA turnover, and these observations raise the key question of how this system regulates RNA metabolism.

Recent proteomic analysis has shown that the deubiquitinating enzyme USP15 is implicated in RNA processing (11). USP15 belongs to the ubiquitin-specific peptidase family and regulates a variety of cellular functions, including mitochondrial homeostasis (12, 13), membrane trafficking from the endoplasmic reticulum (ER) (14), carcinogenesis (15–17), and virus infection (18–20). USP15 deubiquitinates not only lysine 48-linked ubiquitin chains but also lysine 63-linked ubiquitin chains (21). It has been also revealed that USP15 regulates spliceosome assembly (10, 22). In the nervous system, USP15 is expressed in both neurons and glial cells, and aberrant USP15 functions are associated with neuroinflammation and several neurodegenerative disorders, such as ataxia and Parkinson's disease (12, 16, 23). Therefore, it seems that USP15 is required for maintaining brain homeostasis. However, the molecular mechanisms by which USP15 changes RNA metabolism and involves brain homeostasis have not been fully elucidated.

Here, we report that USP15 deubiquitinates terminal uridylyl transferase 1 (TUT1) and regulates the amount of spliceosome component U6 snRNA. We also found that defects in the USP15-TUT1 cascade change global RNA splicing and upregulate chronic ER stress in the cerebellum. Since aberrant RNA splicing causes unusual protein synthesis, our data provide evidence that the USP15-TUT1 cascade is crucial for maintaining brain homeostasis. Thus, our findings suggest a novel mechanism linking abnormal RNA metabolisms to an enhancement of chronic ER stress.

RESULTS

Generation of *Usp15*$^{-/-}$ mice. To understand the physiological functions of USP15, we generated *Usp15*$^{-/-}$ mice (Fig. 1A). USP15 expression was lost in all tissues of *Usp15*$^{-/-}$ mice (Fig. 1B). Interestingly, *Usp15*$^{-/-}$ mice were born at a lower frequency than predicted from a normal Mendelian ratio, conflicting with the previous research (Fig. 1C) (16). One possibility to explain this contradictory result is that the targeting region is distinct from that in the previous study. On the other hand, the life span showed no differences between wild-type (WT) and *Usp15*$^{-/-}$ mice; the majority of *Usp15*$^{-/-}$ mice were able to survive for longer than 2 years despite their growth retardation (Fig. 1D and E). These observations suggest that USP15 is involved in embryogenesis; on the other hand, it has little influence on viability during adulthood.

USP15 is associated with RNA splicing-related factors. Previous studies have suggested that USP15 is implicated in RNA processing and ataxia (11, 23). To verify these hypotheses, we first examined whether USP15 affects global RNA splicing using *Usp15*$^{-/-}$ cerebellum. The global gene expression patterns in *Usp15*$^{-/-}$ cerebellum were changed from those in the wild type (21 genes in the cerebellum, fold change $>$ 1.5, $P < 0.05$) (see Table S1 in the supplemental material). On the other hand, the splicing changes in *Usp15*$^{-/-}$ were relatively high (245 genes in the cerebellum, splicing index [SI] fold change > 0.5; $P < 0.05$) (Fig. 2A and Table S2), indicating that USP15 influences the global profiling of RNA splicing. Next, to investigate the molecular mechanisms by which USP15 regulates RNA processing, we explored the target proteins using liquid chromatography-tandem mass spectrometry (LC-MS/MS). Consistent with the previous study, we identified several USP15-interacting proteins, such as TUT1,

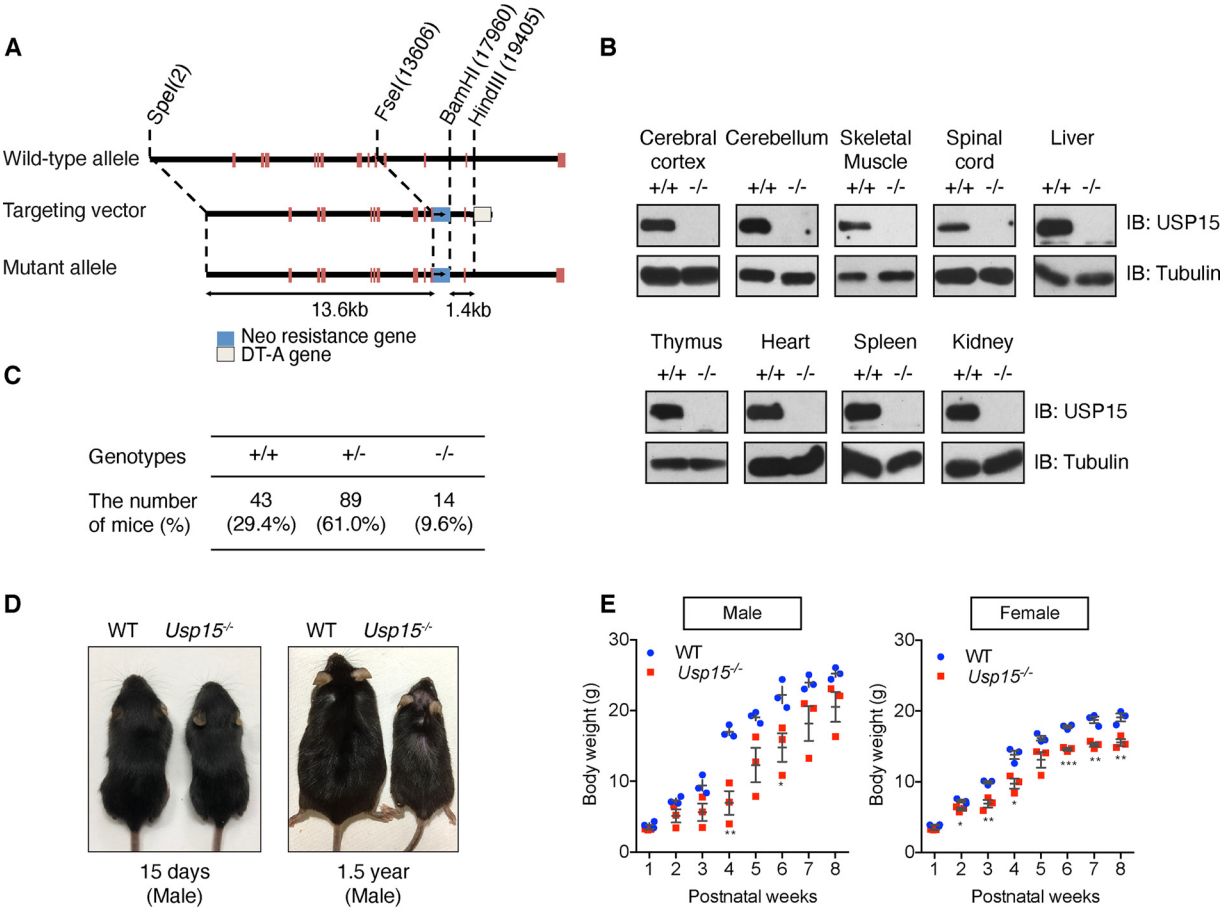

FIG 1 Generation of *Usp15*$^{-/-}$ mice. (A) Schematic representation of mouse *Usp15* gene (wild-type allele), targeting vector, and mutant gene (mutant allele). Neo, neomycin; DT-A, diphtheria toxin gene. (B) Immunoblotting of USP15 and tubulin in the supernatant of indicated organs derived from wild-type and *Usp15*$^{-/-}$ littermate mice at P90. (C) Genotype frequencies of postnatal mice (approximately P7) produced from *Usp15*$^{+/-}$ mouse intercrosses. (D) Representative image of wild type and *Usp15*$^{-/-}$ mice. P15 and 1.5-year-old littermates are shown. (E) Body weights of male and female wild-type and *Usp15*$^{-/-}$ littermate mice were measured from P7 to week 8. Each point includes data from three individuals. $n = 3$; mean ± standard error of the mean (SEM); *, $P < 0.05$; **, $P < 0.01$; ***, $P < 0.005$ by Student's *t* test.

SART3, and LSm proteins (11) (Fig. 2B). It is known that SART3 promotes U4/U6 snRNP assembly and TUT1 uridylates at the 3′ of U6 snRNA, followed by recruitment of LSm proteins (Fig. 2C). Thus, these proteins may become prepotent candidates that regulate RNA splicing related to USP15. To verify whether USP15 binds to these proteins, we performed a coimmunoprecipitation assay. In accord with the previous studies, SART3 and TUT1 coprecipitated with USP15 (11, 24, 25) (Fig. 2D and E). In contrast, we did not detect clear binding between USP15 and LSm proteins, such as LSm2 and LSm6 (Fig. 2F). Thus, we presumed that USP15 is not incorporated into the U6 snRNA complex but modulates its function or that the binding affinity toward LSm proteins is weak. As USP15 binds to both SART3 and TUT1, we speculated that these proteins form the ternary complex. Indeed, TUT1 interacted with SART3 (Fig. 2G). In addition, the interaction between USP15 and TUT1 became stronger when SART3 was coexpressed (Fig. 2E), suggesting that SART3 enhances the association of USP15 with TUT1. As USP15 interacts with SART3 through the HAT repeat domain (residues 278 to 611) (22), we examined which region of SART3 is important for interacting with TUT1 by dividing SART3 into two fragments (Fig. 2H). The N-terminal fragment (residues 1 to 649) did not interact with TUT1, but the C-terminal fragment (residues 660 to 963) associated with it, indicating that the C-terminal region of SART3 is the binding region to TUT1 (Fig. 2I). Next, we investigated whether overexpression of the C-terminal fragment hampers an interaction between USP15 and TUT1. As expected, SART3$^{660-963}$ deletion decreased

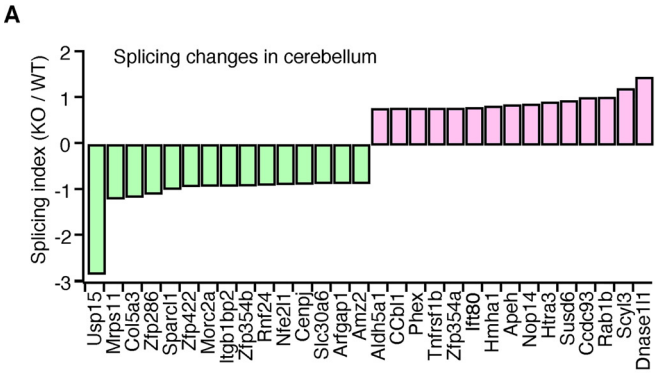

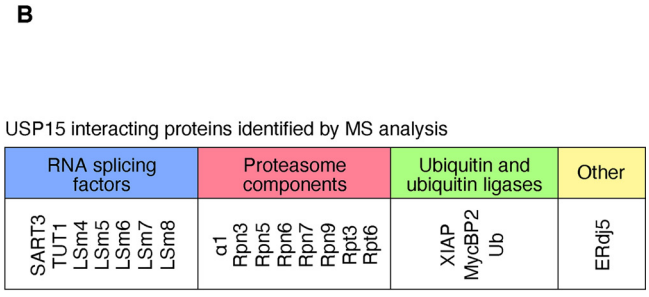

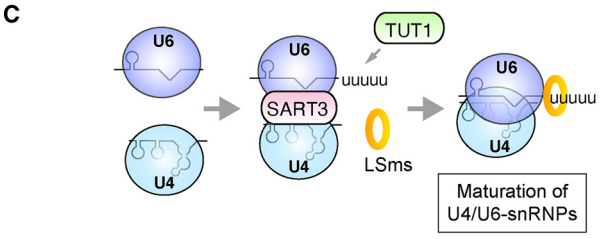

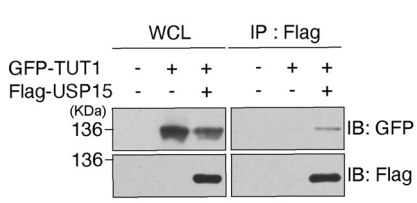

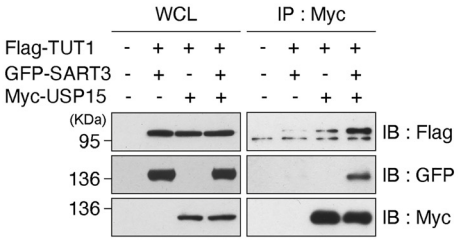

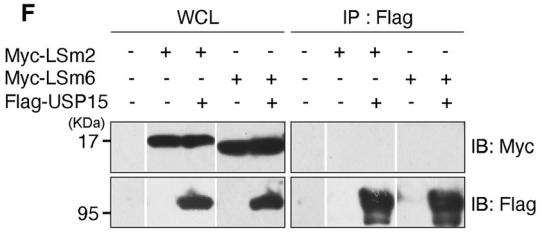

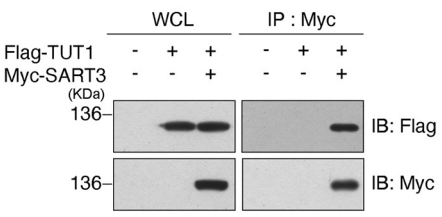

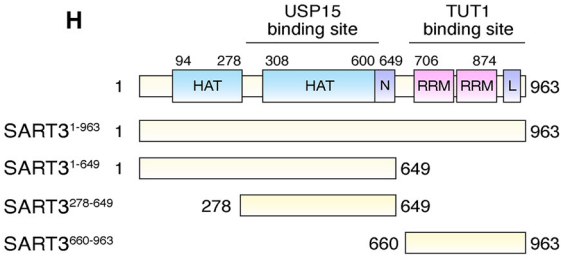

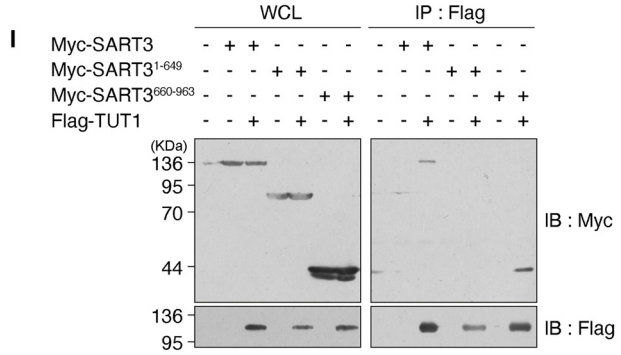

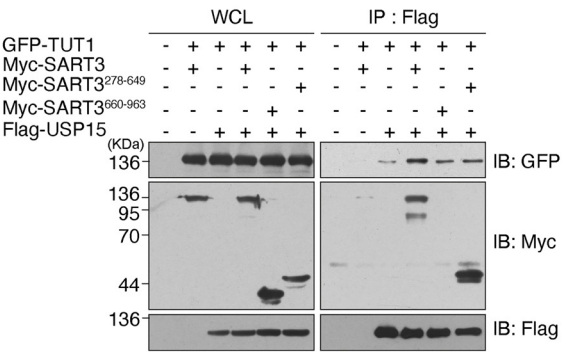

FIG 2 USP15 is associated with RNA splicing-related factors. (A) Variations of splicing patterns identified in exon array analysis. The graph indicates the top 15 genes (upregulation and downregulation) of the splicing index from the cerebellum affected by *Usp15* deficiency. (B) USP15-interacting proteins identified by MS analysis. (C) Model for the maturation of U4/U6 snRNP spliceosome. TUT1 uridylates at the 3′ of U6 snRNA. SART3 promotes interaction between U6 snRNP and U4 snRNP. LSm proteins interact with the 3′ region of U6 snRNA. (D) Coimmunoprecipitation of Flag-USP15 and GFP-TUT1 in HEK293 cells. Flag-USP15 was immunoprecipitated with an anti-Flag antibody and immunoblotted with anti-GFP and anti-Flag antibodies. (E) Coimmunoprecipitation of Flag-TUT1 and Myc-USP15 with coexpression of either GFP-SART3 or control in HEK293T cells. Proteins were immunoprecipitated with anti-Myc antibody and immunoblotted with anti-Flag, anti-GFP, and anti-Myc antibodies. (F) Myc-LSm2, Myc-Lsm6, and Flag-USP15 were immunoprecipitated with anti-Flag antibody and immuno-

(Continued on next page)

the interaction between USP15 and TUT1. Also, SART3$^{278-649}$ reduced their interaction (Fig. 2J), implying that SART3 acts as a potential scaffold protein for enhancing the interaction of USP15 with TUT1.

USP15 deubiquitinates TUT1. We next examined whether USP15 deubiquitinates TUT1 and SART3. Coexpression of USP15 clearly reduced the amount of ubiquitinated TUT1, while that of the USP15 D879A mutant, which lacks its enzyme activity, did not (Fig. 3A). In the *in vitro* deubiquitination assay, recombinant USP15 also reduced polyubiquitination on TUT1 (Fig. 3B and C). On the other hand, we could not detect enough polyubiquitin chains on SART3 under basal conditions. However, a small amount of SART3 monoubiquitylation was detected, and this modification was reduced by USP15 expression (Fig. 3D). These data imply that TUT1 is the main target protein by USP15. Given that SART3 facilitates the interaction between USP15 and TUT1, it is likely that SART3 also promotes USP15-induced TUT1 deubiquitination. Practically, the coexpression of SART3 with USP15 promoted TUT1 deubiquitination (Fig. 3E). Furthermore, expression of the SART3 deletion mutant, which hampers an interaction between USP15 and TUT1, partially canceled USP15-related deubiquitination of TUT1 (Fig. 3F), suggesting that SART3 served as a substrate targeting factor of USP15. Recently, it has been reported that USP15 is in charge of deubiquitination for not only K48-linked but also K63-linked ubiquitin linkage (21). Therefore, we examined which ubiquitin linkage on TUT1 is deubiquitinated by USP15. To test this, we used the ubiquitin K48R and K63R mutants, of which residues K48 and K63 are mutated to arginine, and 48K and 63K, of which all lysine residues are mutated to arginine except at K48 and K63, respectively. TUT1 was ubiquitinated by the WT and K48R and 63K mutants, exclusively. Moreover, coexpression of USP15 reduced the amount of ubiquitinated TUT1, demonstrating that USP15 deubiquitinates K63-linked ubiquitin chains on TUT1 (Fig. 3G). Notably, the ubiquitination level by the K48R mutant was higher than that by the WT. We presume that TUT1 turnover could be fast under the basal condition, and accordingly, the K48R mutant delays this reaction. Together, these data suggest that USP15 deubiquitinates K63 ubiquitin linkage of TUT1, and SART3 accelerates the deubiquitinating reaction.

USP15 controls the amount of U6 snRNA associated with TUT1. To determine the physiological role of the deubiquitination of TUT1, we investigated whether overexpression of USP15 alters TUT1 subcellular localization. Consistent with the previous studies (26, 27), TUT1 was generally localized in the nucleolus in HeLa cells (Fig. 4A). However, overexpressed USP15 redistributed TUT1 from the nucleolus to the nucleoplasm (Fig. 4B to D). SART3 is reported to redistribute USP15 into the nucleus by nuclear localization signals and is thereby involved in the deubiquitinating efficiency of USP15 toward target protein in the nucleus (24). As SART3 enhanced an association of USP15 with TUT1 as shown in Fig. 2E, we supposed that SART3 has a similar role in regulating TUT1 subnuclear localization by changing USP15 localization. Indeed, SART3 recruited USP15 into the nucleus and elevated TUT1 translocation to the nucleoplasm (Fig. 4C and D). Given that SART3 promotes USP15 deubiquitinating efficiency on TUT1, deubiquitination by USP15 associated with SART3 may regulate the subnuclear localization of TUT1. Next, we tested whether USP15 is necessary for regulating the localization of TUT1 using *Usp15*$^{-/-}$ mouse embryonic fibroblasts (MEFs). Unexpectedly, TUT1 localized mainly in the nucleoplasm and was not redistributed to the nucleolus even in *Usp15*$^{-/-}$ MEFs (Fig. 4E and F). These data indicate that USP15 is sufficient but not necessary for regulating TUT1 subnuclear localization and imply that another pathway exists in cells (see Discussion).

FIG 2 Legend (Continued)
blotted with anti-Flag and anti-Myc antibodies. (G) Coimmunoprecipitation of Flag-TUT1 and Myc-SART3 in HEK293 cells. Proteins were immunoprecipitated with anti-Myc antibody and immunoblotted with anti-Flag and anti-Myc antibodies. (H) Schematic structure of SART3. HAT, half-a-tetratricopeptide repeats; N, nuclear localization signal; RRM, RNA recognition motif; L, LSm binding region. (I) Coimmunoprecipitation of Flag-TUT1 and either Myc-SART3 or Myc-SART3 deletion mutants in HEK293T cells. Proteins were immunoprecipitated with an anti-Flag antibody and immunoblotted with anti-Myc and anti-Flag antibodies. (J) Coimmunoprecipitation of Flag-USP15 and GFP-TUT1 when either Myc-SART3 or Myc-SART3 deletion mutants was coexpressed in HEK293T cells. Proteins immunoprecipitated with an anti-Flag antibody were immunoblotted with anti-GFP, anti-Myc, and anti-Flag antibodies.

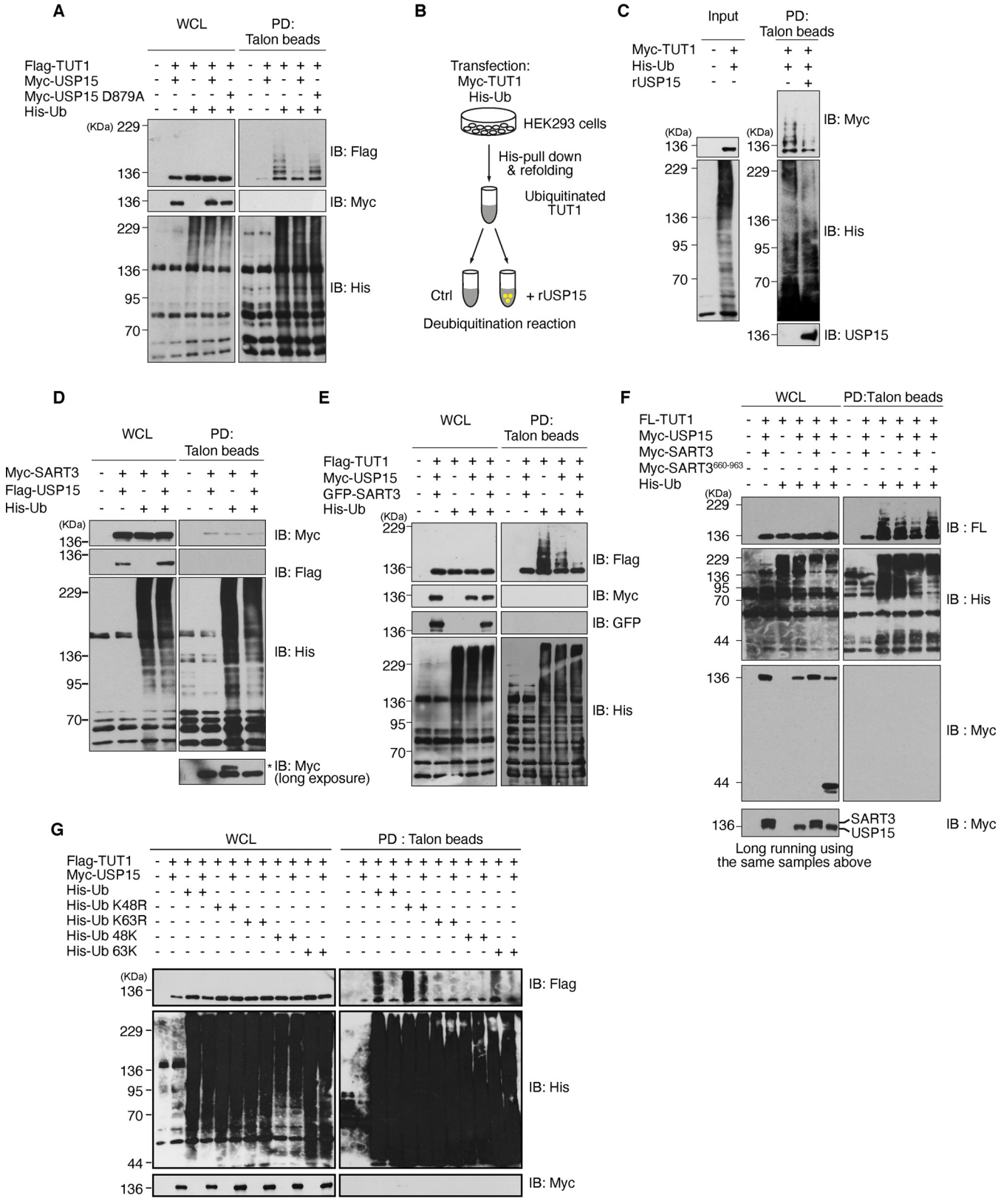

FIG 3 USP15 deubiquitinates TUT1. (A) Ubiquitinated proteins from HEK293 cells expressing Flag-TUT1, Myc-USP15, or Myc-USP15 D879A and His-Ub were pulled down with Talon metal affinity resin and immunoblotted with anti-Flag, anti-Myc, and anti-His antibodies. (B and C) *In vitro* deubiquitination of TUT1. (B) A schematic diagram of isolation of ubiquitinated Myc-TUT1 and deubiquitination reaction with USP15. (C) His-ubiquitinated TUT1 was pulled down with Talon metal affinity resin from HEK293 cells expressing Myc-TUT1 and His-Ub, incubated with recombinant USP15 (LifeSensors) for deubiquitination reaction, and analyzed by immunoblotting with anti-Myc, anti-USP15, and anti-His antibodies. (D) Flag-USP15, Myc-SART3, and His-Ub were pulled down with Talon metal

(Continued on next page)

Since the substrates of TUT1, such as U6 snRNA, mainly exist in the nucleoplasm, we presumed that TUT1 in the nucleoplasm plays an important role in the modification of U6 snRNA. To verify this, we first analyzed a nucleotidyltransferase activity of TUT1 by using a polyadenylation assay. Immunoprecipitated TUT1-mediated adenylation levels were reproducibly increased when TUT1 was coexpressed with USP15 (Fig. 4G), implying that the deubiquitination of TUT1 increases enzymatic activity. As TUT1 is known to modify U6 snRNA (26, 28), we hypothesized that TUT1 deubiquitination influences the U6 snRNA level in cells. To test this, we analyzed the amount of U6 snRNA in the presence or absence of TUT1, USP15, and SART3. The U6 snRNA was upregulated when both TUT1 and USP15 were coexpressed, whereas the U6 snRNA level was slightly decreased by coexpression of USP15 D879A (Fig. 4H), suggesting that USP15 and TUT1 are sufficient for maintaining U6 snRNA levels. We next examined if TUT1 knockdown reduces the amount of U6 snRNA conversely. To do this, we used TUT1 small interfering RNAs (siRNAs) (Fig. 4I). As expected, TUT1 knockdown decreased the amount of U6 snRNA (Fig. 4J), suggesting that TUT1 is necessary for controlling the amount of U6 snRNA. We next examined whether the amount of U6 snRNA is decreased in the *Usp15*$^{-/-}$ brain. The U6 snRNA levels were moderately but significantly lower in the *Usp15*$^{-/-}$ brain than in the WT brain (Fig. 4K and L). These data suggest that USP15 augments the U6 snRNA level by regulating TUT1 activity.

Loss of USP15 impairs cerebellar maintenance. Substantial studies have reported that defects in several RNA splicing-related factors, including U snRNAs, cause motor dysfunctions and neurodegeneration (2, 29–31). Also, U6 snRNA prevents cell death from a defect in RNA splicing factors (32). Thus, we predicted that loss of the *Usp15* gene results in motor dysfunctions and a neurodegenerative phenotype. To investigate this, we analyzed the motor ability tests of *Usp15*$^{-/-}$ mice. *Usp15*$^{-/-}$ mice exhibited motor defects, such as tremor and abnormal hind limb clasping reflexes in older mice (Fig. 5A). In a rotarod test, *Usp15*$^{-/-}$ mice tended to grasp the rod instead of walking on the rotating rod and fell to the ground earlier than wild-type mice (Fig. 5B and C), suggesting that loss of USP15 impairs motor coordination. As motor disorders result from dysfunctions of the cerebellum, we next performed anatomical and histological analyses of *Usp15*$^{-/-}$ cerebellum. In *Usp15*$^{-/-}$ cerebellar vermes, impaired foliation was evident at lobule crus 3 and 8 (Fig. 5D). Since USP15 was dominantly expressed in Purkinje cells (Fig. 5E), we next examined whether Purkinje cells were affected by the loss of USP15. The size of Purkinje cells in the *Usp15*$^{-/-}$ cerebellum was gradually reduced over time (Fig. 5F and G). As the reduction in the size of Purkinje cells is tightly linked to the neurodegenerative phenotype (33, 34), we investigated whether a loss of *Usp15* causes neurodegeneration in an age-dependent manner. Consequently, active caspase-3 was slightly increased in the Purkinje layer of 4-month-old cerebellum (Fig. 5H). Furthermore, the Purkinje cells in the *Usp15*$^{-/-}$ cerebellum showed a neurodegenerative phenotype at 1.5 years old (Fig. 5I), indicating that USP15 is required for the integrity of Purkinje cells.

Defects in the USP15-TUT1 cascades enhance chronic and mild ER stress. The remaining question is how *Usp15* deficiency results in developmental defects in an age-dependent manner. Since USP15 is implicated in ER homeostasis (14, 35, 36), we next analyzed whether the USP15-TUT1 cascade is involved in ER stress linked to neuronal defects. It has been known that ER stress increases with age and neurode-

FIG 3 Legend (Continued)
affinity resin and immunoblotted with anti-Flag, anti-Myc, and anti-His antibodies. The asterisk indicates a putative monoubiquitinated SART3. (E) Precipitation of His-Ub-conjugated Flag-TUT1 in the presence or absence of Myc-USP15 and GFP-SART3. Ubiquitinated proteins from HEK293 cells expressing Flag-TUT1, Myc-USP15, GFP-SART3, and His-Ub were pulled down using Talon metal affinity resin and immunoblotted with anti-Flag, anti-Myc, anti-GFP, and anti-His antibodies. (F) Ubiquitinated proteins from HEK293 cells expressing Flag-USP15, Myc-SART3, Myc-SART3$^{660–963}$ deletion mutant and His-Ub were pulled down with Talon metal affinity resin and immunoblotted with anti-Flag, anti-Myc, and anti-His antibodies. The bottom panel shows a different mobility shift against Myc-USP15 and Myc-SART3. These samples were separated by extended electrophoresis using the same samples as in the top panels. (G) Precipitation of wild-type or mutant His-Ub-conjugated Flag-TUT1 in the presence or absence of Myc-USP15. Ubiquitinated proteins from HEK293 cells expressing Flag-TUT1, Myc-USP15, and either wild-type or mutant His-Ub were pulled down with Talon metal affinity resin and immunoblotted with anti-Flag, anti-Myc, and anti-His antibodies.

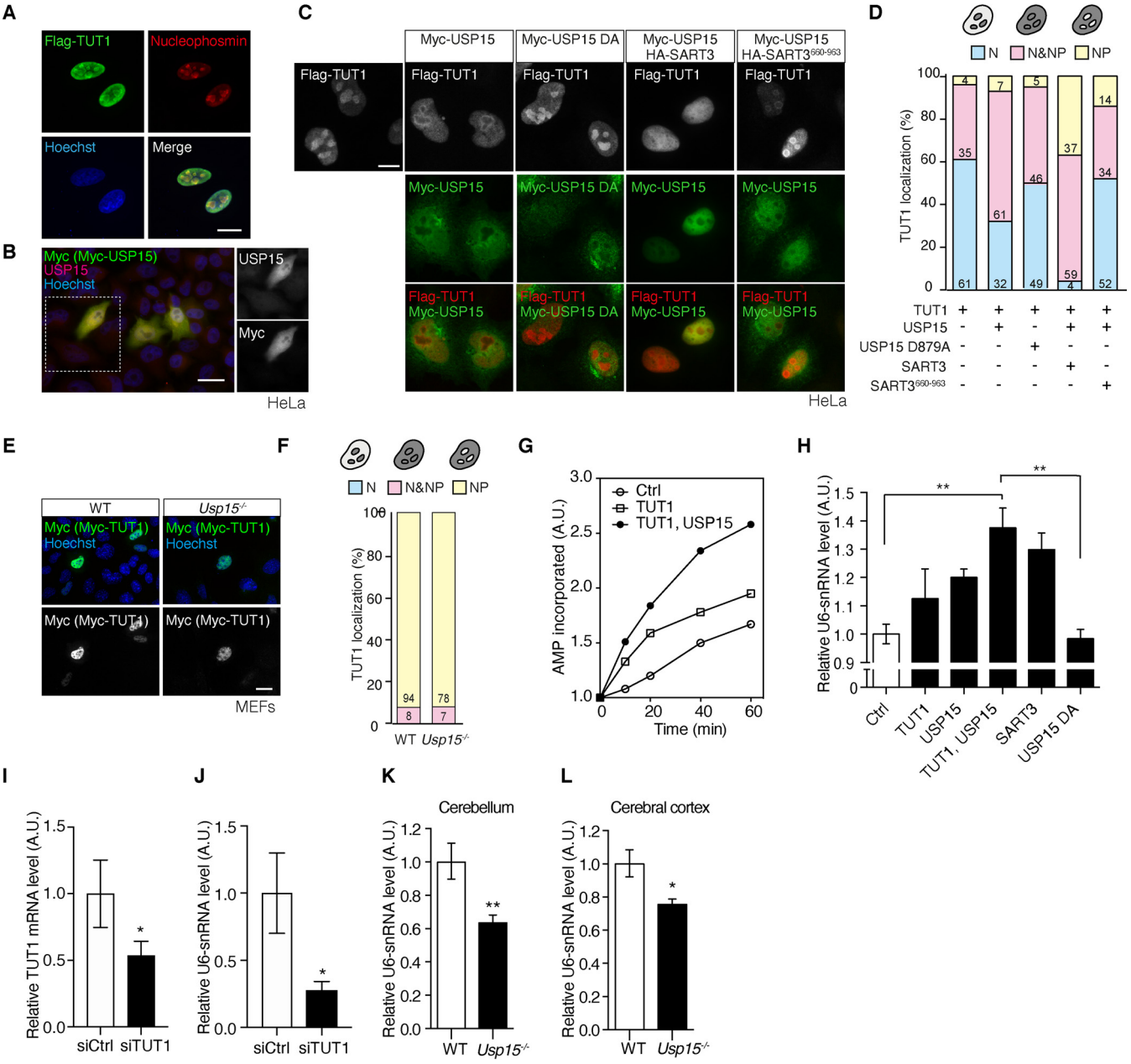

FIG 4 USP15 controls the amount of U6 snRNA associated with TUT1 activity. (A) Immunostaining of Flag-TUT1 in HeLa cells. The cells were immunostained with a nucleolus marker, antinucleophosmin antibody. Scale bar, 20 μm. (B) Immunostaining of Myc-USP15 in HeLa cells. The cells were immunostained with anti-Myc and anti-USP15 antibodies. Scale bar, 20 μm. The fluorescence intensity (FI) of overexpressed Myc-Usp15 is 2.42-fold higher than that of endogenous USP15 (FI of endogenous USP15, 13.21 $\pm$ 1.97; FI of overexpressed USP15, 31.95 $\pm$ 4.76; mean $\pm$ SEM, $n = 45$, $P < 0001$ by Student's t test). (C) Immunofluorescence of Flag-TUT1 together with Myc-USP15, Myc-USP15 D879A, HA-SART3, and HA-SART3$^{660-963}$ in HeLa cells. Scale bar, 20 μm. (D) Quantification of the data shown in panel C. Flag-TUT1 in the nucleolus (N), both nucleolus and nucleoplasm (N&NP), or the nucleoplasm (NP) were counted. $n = 100$. (E) Immunofluorescence of Myc-TUT1 in MEFs. Scale bar, 20 μm. (F) Quantification of the data shown in panel E. Myc-TUT1 in the nucleolus (N), both nucleolus and nucleoplasm (N&NP), or the nucleoplasm (NP) were counted in MEFs. WT, $n = 102$; knockout (KO), $n = 85$. (G) Polyadenylation activity of TUT1. Recombinant TUT was immunoprecipitated with an anti-Flag antibody from HEK293T cells expressing Flag-TUT1 only or Flag-TUT1 and Myc-USP15 and subjected to polyadenylation reaction using [α-^{32}P]ATP. ^{32}P-labeled AMP incorporation was measured by liquid scintillation counting. (H) U6 snRNA levels in HEK293 cells expressing indicated plasmids. U6 snRNA levels were measured by qPCR and normalized with the 5S rRNA level. The bar graph shows the fold changes each sample relative to control. $n = 3$; mean $\pm$ SD; **, $P < 0.01$ by one-way ANOVA. (I) Total RNAs isolated from the HEK293T cells were reverse transcribed and subjected to qPCR analysis for measurement of mRNA levels of TUT1. mRNA levels of 5S rRNA were used for normalization. $n = 4$; mean $\pm$ SEM; *, $P < 0.05$ by Student's t test. (J) U6 snRNA levels affected by TUT1 knockdown. The RNAs were purified from HEK293T cells transfected with control or siTUT1 and reverse transcribed. U6 snRNA levels were measured by qPCR and normalized with 5S rRNA levels. $n = 3$; mean $\pm$ SEM; *, $P < 0.05$ by Student's t test. U6 snRNA levels in wild-type and *Usp15*$^{-/-}$ cerebellum (K) and cerebral cortex (L). The RNAs were isolated from wild-type and *Usp15*$^{-/-}$ brain obtained from 3-month-old female littermate mice and subjected to reverse transcription. 5S rRNA levels were used for normalization. $n = 4$; mean $\pm$ SD; *, $P < 0.05$; **, $P < 0.01$ by Student's t test.

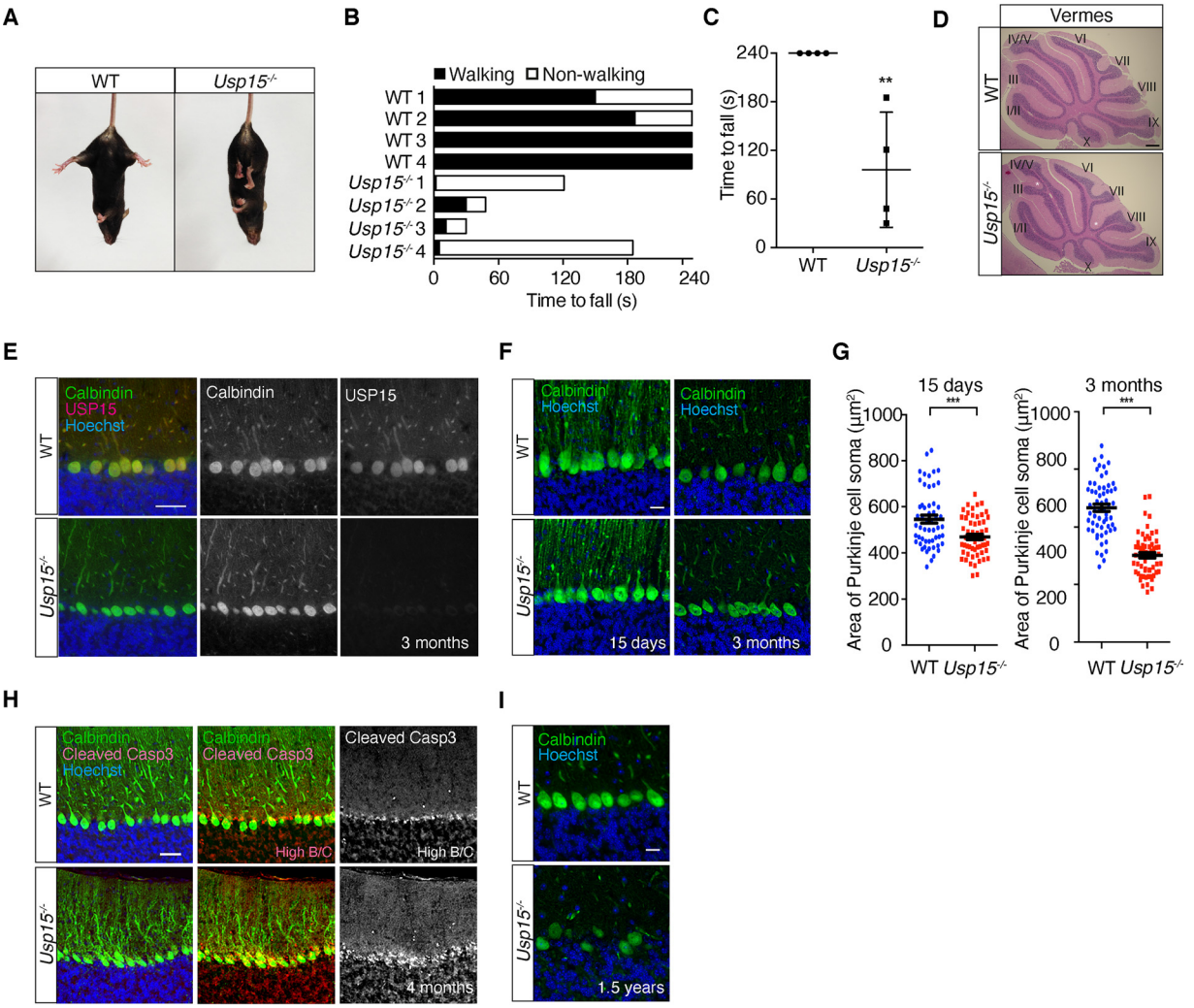

FIG 5 Loss of USP15 impairs cerebellar maintenance. (A) Abnormal hind limb clasping reflexes of *Usp15*$^{-/-}$ mouse compared to that of wild-type mouse in tail suspension test; 3-month-old littermates. (B and C) Rotarod testing of wild-type ($n = 4$) and *Usp15*$^{-/-}$ mice ($n = 4$); 2-month-old littermates. (B) The riding time of each mouse on a rotating rod was measured. Black bars indicate the time walking on the rod and white bars indicate time spent grasping the rod instead of walking. (C) The total time spent on the rod was measured. The graph shows means ± standard deviations (SDs). **, $P < 0.01$ by Student's *t* test. (D) Histological analyses of wild-type and *Usp15*$^{-/-}$ cerebellar vermes at P83. Paraffin sections were stained with hematoxylin and eosin. Asterisks indicate abnormal foliation of lobules; 3-month-old littermates were used. This phenotype was consistently observed in at least three independent mice. Scale bar, 200 μm. (E) Immunohistochemical analyses of wild-type and *Usp15*$^{-/-}$ cerebellums at 3 months old. The brain sections were immunostained with anti-USP15 and anticalbindin antibodies. Scale bar, 20 μm. (F) Immunohistochemical analyses of wild-type and *Usp15*$^{-/-}$ cerebellums. Fifteen-day- and 3-month-old mouse cerebellums of each genotype were used. The brain sections were immunostained with an anticalbindin antibody. Scale bar, 50 μm. (G) Quantification of the size of Purkinje cell somas in 15-day- and 3-month-old mice. $n = 55$ (15 days) and $n = 60$ (3 months); mean ± SEM. ***, $P < 0.005$ by Student's *t* test. The immunohistochemical images present the representative results from two independent experiments. (H) Immunohistochemical analyses of wild-type and *Usp15*$^{-/-}$ cerebellums from 4-month-old mice. The brain sections were immunostained with anti-cleaved caspase-3 and anticalbindin antibodies. High B/C, increasing brightness and contrast. Scale bar, 20 μm. (I) Immunohistochemical analyses of wild-type and *Usp15*$^{-/-}$ cerebellums of 1.5-year-old mice from each genotype. The brain sections were immunostained with an anticalbindin antibody. Scale bar, 50 μm.

generative disorders over time (37, 38). In addition, ER stress acts in concert with RNA splicing and is associated with the redistribution of splicing factors (39, 40). Furthermore, mutations in the membrane and secretory proteins are thought to elicit the accumulation of their translational products in the ER (41–44). These studies prompted us to investigate whether the USP15-TUT1-spliceosome cascade is involved in ER stress. To examine this, we first analyzed the sensitivity to ER stress using *Usp15*$^{-/-}$ MEFs. In consequence, the timing of cell death induced by ER stresses was delayed in *Usp15*$^{-/-}$ MEFs compared to that in WT MEFs (Fig. 6A), implying that *Usp15*$^{-/-}$ MEFs are resistant to an acute and severe ER stress. It seems that a mild stimulation, which does not

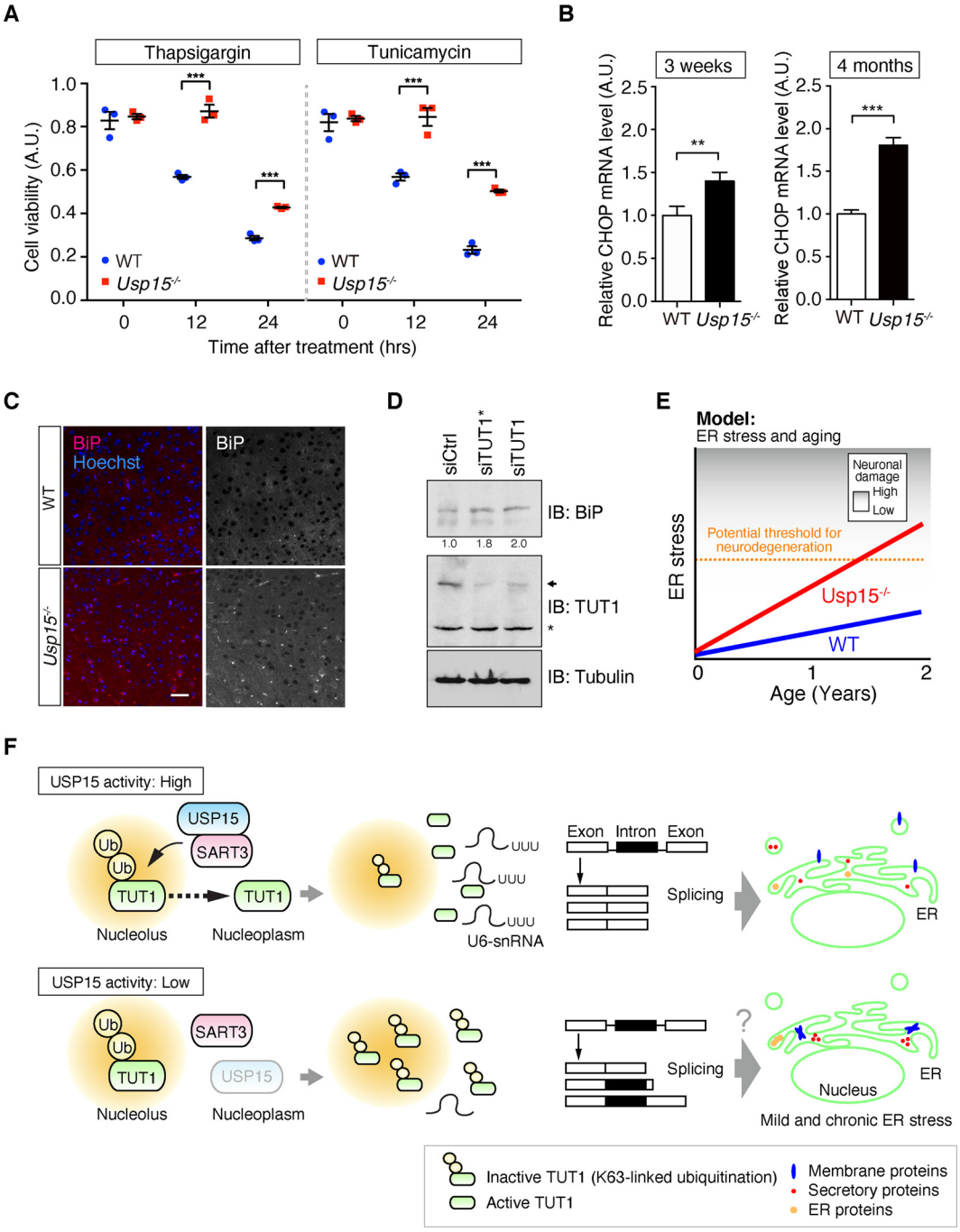

FIG 6 Defects in the USP15-TUT1 cascade enhance chronic and mild ER stress. (A) MEFs were stimulated with 300 nM thapsigargin (left) and 1.0 μg/ml tunicamycin (right) for the indicated times. The cellular viability was analyzed using the Cell Counting Kit-8 ($n = 3$, means $\pm$ SEM; ***, $P < 0.005$ by Student's t test). (B) The mRNA of CHOP in wild-type and *Usp15*$^{-/-}$ cerebellum. The RNAs were isolated from wild-type and *Usp15*$^{-/-}$ cerebellums obtained from 3-week-old and 4-month-old mice and subjected to reverse transcription. 5S rRNA levels were used for normalization. $n = 3$; mean $\pm$ SD; **, $P < 0.01$; ***, $P < 0.005$ by Student's t test. (C) Immunohistochemical analyses of wild-type and *Usp15*$^{-/-}$ cerebral cortex; 1.5-year-old mice were used. The brain sections were immunostained with an anti-BiP antibody. Scale bar, 50 μm. (D) TUT1 siRNA treated HEK293T cell lysates were immunoblotted with anti-TUT1 and antitubulin antibodies. The numbers indicate the ratio of BiP to tubulin. Arrow, TUT1 bands; asterisk, nonspecific bands (E) Conceptual diagram for a relationship between ER stress and aging. (F) USP15 deubiquitinates TUT1 concerted with SART3, contributing to the U6 snRNA stabilization. A defect in USP15 disturbs RNA splicing and produces aberrant proteins, increasing mild and chronic ER stress.

induce cell death, can reduce damage triggered by subsequent severe stimulation in the brain (45). Probably, mild and chronic ER stress enables cells to resist subsequent severe stress. Next, to investigate a link between USP15-TUT1 and ER stress, we analyzed the expression of the ER stress marker CHOP in the *Usp15*$^{-/-}$ cerebellum. As expected, CHOP expression was upregulated in *Usp15*$^{-/-}$ brain with age (Fig. 6B), suggesting that a defect in USP15 enhances mild ER stress, leading to an increase of CHOP expression even under the basal conditions. To further confirm that ER stress is increased in *Usp15*$^{-/-}$ brain with age, we stained *Usp15*$^{-/-}$ brain sections with an anti-BiP antibody. Expression of BiP clearly increased in the *Usp15*$^{-/-}$ brain (Fig. 6C). Finally, we investigated whether TUT1 is involved in the upregulation of ER stress. Treatment of HEK293T cells with TUT1 siRNA increased the BiP expression level (Fig. 6D), demonstrating that dysfunctions of TUT1 enhance ER stress. Taken together, our data suggest that defects in both USP15 and TUT1 augment the basal level of ER stress associated with aging.

DISCUSSION

In this study, we identified TUT1 as a novel target of USP15. USP15 alters TUT1 subnuclear localization and activity through its deubiquitination, followed by a change in global RNA metabolism. We also found that *Usp15* deficiency increases ER stress and results in aberrant motor functions in an age-dependent manner. Since inhibition of the USP15-TUT1 cascade enhances ER stress, our findings suggest a novel mechanism that links spliceosome dysfunctions to ER stress induction with age (Fig. 6E and F).

So far, it has been reported that USP15 deubiquitinates several splicing factors, such as PRP31 and PRP3, in concert with SART3 (10). PRP31 and PRP3 constitute core elements of U6 snRNA and are crucial for regulating RNA splicing. Indeed, the ubiquitination of these proteins plays an important role in U4/U6.U5 snRNP assembly (9). Therefore, it is likely that PRP31 and PRP3 are the interesting candidates associated with USP15-dependent RNA splicing. In this study, we also identified another target, TUT1. TUT1 is known to add a short uridine tail to the 3′ end of U6 snRNA, which is a core noncoding RNA in the spliceosome. This uridylation recruits LSm proteins and confers the proper functions of the U6 snRNP complex (Fig. 2C) (46). Therefore, we presume that TUT1 and SART3 also act as potential mediators that link USP15 to RNA splicing in addition to the PRP cascade. Intriguingly, we observed that overexpression of USP15 deubiquitinates SART3, although the proportion was markedly low under the basal condition. As USP15 has been reported to eliminate monoubiquitylation of receptor-regulated Smad (R-Smad) and regulate transforming growth factor β (TGF-β) signaling (47), monoubiquitinated SART3 could be regulated by USP15 and affect the RNA metabolic pathway. We also observed that a loss of *Usp15* does not affect TUT1 subnuclear localization in MEFs. So far, we already found that USP4, which is a homolog of USP15, also deubiquitinates TUT1, leading to altered subnuclear localization (unpublished data). Since USP4 has a common substrate for USP15 (9, 10), it is likely that USP15 is not the sole deubiquitinating enzyme, and the basal activity of USP4 could be higher than that of USP15 in MEFs. Another question is the physiological significance of TUT1 in the nucleolus. Interestingly, a loss of *Usp15* decreased the amount of U6 snRNA in not only the brain (Fig. 4K and L) but also MEFs (unpublished data). On the other hand, the overexpression of USP15 promoted TUT1 activity in an *in vitro* assay (Fig. 4G). Thus, we predict that the deubiquitination of TUT1 has two physiological meanings. First, deubiquitination promotes TUT1 redistribution to the nucleoplasm in a cell-specific manner. Second, TUT1 deubiquitination increases an enzymatic activity of itself. Consequently, it seems that deubiquitinated TUT1 modifies U6 snRNA in the nucleoplasm and then stabilizes it. However, the precise molecular mechanisms will need to be considered more carefully in the future.

Previously, several groups have reported that U snRNAs are implicated in maintaining brain functions. Mutation in U2 snRNA causes cerebellar granule cell degeneration by reducing the splicing efficiency (48). In addition, abnormal accumulation of U1 snRNP is implicated in the pathogenesis of Alzheimer's disease (49). Furthermore, a

mutation in SMN, which is essential for U snRNA assembly and RNA splicing, causes spinal muscular atrophy (SMA) (50, 51). We observed a change in the amount of U6 snRNA triggered by USP15 inhibition and abnormality of both cerebellar morphogenesis and Purkinje cell maintenance in *Usp15*$^{-/-}$ mice. Since spliceosome deficiency increases neuronal cell death, a defect in the USP15-TUT1-U6 snRNA cascade results in perturbed cerebellar maintenance. The interesting question is how the loss of USP15 accelerates this phenotype. It has been reported that mutations in secretory proteins and membrane proteins induce ER stress via abnormal membrane trafficking (41–44). Indeed, we observed that USP15 deficiency produces various mutants produced by splicing errors, followed by an increase in chronic ER stress in an age-dependent manner. As neurons are vulnerable to such ER stresses and a prolonged stress response leads to neuronal cell death (38), it is possible that cerebellar abnormality in *Usp15*$^{-/-}$ is accelerated by ER stress-induced damage accumulation. Here, we identified several intriguing candidates from a set of exon array analyses. One interesting target is Sparcl1, which is a secreted protein from astrocytes that enhances synapse connections (52). We have already identified the splicing variant of Sparcl1 from *Usp15*$^{-/-}$ brain. Our preliminary data suggest that these variants accumulate in the ER and are attenuated in their secretion efficiency due to aberrant membrane trafficking. Because USP15 is expressed in not only neurons but also astrocytes, the onset of glioblastoma caused by aberrant USP15 functions may be linked to an accumulation of unusual splicing variants in the ER, promoting neuroinflammation. The other interesting target is the *Nrf1/Nfe2l1* gene. A previous study reported that a defect in the *Nrf1* gene triggers cerebellar degeneration, which is similar to the phenotype of *Usp15*$^{-/-}$ mice (53). It is also known that NRF1 is associated with ER stress response and is deubiquitinated by USP15 (36, 54). Thus, *Nrf1* splicing variants produced by *Usp15* deficiency could be an intriguing candidate that exhibits the phenotype of *Usp15*$^{-/-}$ mice.

We consider that USP15 functions are influenced by posttranslational modification and alternative splicing. A recent study reported that USP15 phosphorylation is crucial for regulating the subcellular localization of USP15. Human USP15 is phosphorylated at Thr149 and Thr219 and prevents binding with SART3, resulting in the sequestration of USP15 from the nucleus (55). It has also been reported that USP15 possesses a splicing variant, which lacks exon 7 regions. This exon 7 often acts as a target recognition site. The specificity toward the target proteins is distinct between the regular form and an exon 7-lacking form (56). Moreover, the region of exon 7 has several phosphorylation sites (55) (www.phosphosite.org), indicating that posttranslational modification and synthesis of splicing variants are the key processes that underlie the regulation of USP15 functions. Thus, the target specificity of USP15 could be controlled by the existence of exon 7 or its phosphorylation, contributing to mRNA diversity. So far, the aging and neurodegenerative phenotypes have been known to be associated with the activation of several kinases, such as Jun N-terminal protein kinase (JNK) (37). Thus, these kinases associated with aging may be a potential candidate for the phosphorylation of USP15.

In summary, we propose that the USP15-TUT1 cascade changes global RNA metabolism. USP15 deubiquitinates TUT1, contributing U6 snRNA stability and spliceosome function. A defect in the USP15-TUT1 cascade enhances ER stress and the neurodegenerative phenotype. This finding reveals important mechanisms for USP15-TUT1 and sheds light on the new approaches to understand how abnormal RNA turnover links to disturbed brain homeostasis.

MATERIALS AND METHODS

Animals. All animal experiments were conducted according to the University of Tsukuba guidelines for animal care and use (approval numbers 17-302, 18-257, and 19-340). The generation of knockout mice was as follows. The *Usp15* gene was obtained from the mouse BAC library. The targeting vector was constructed by insertion of the genomic DNA containing the neomycin resistance gene into SpeI and HindIII sites. The diphtheria toxin gene (DT-A gene) was attached to the 3′ end of the *Usp15*-neomycin construct (Fig. 1A). The targeting vector was electroporated into TT2 embryonic stem (ES) cells. After selection with G418 (Sigma), the ES cells heterozygous for the *Usp15* gene were microinjected into eight-cell-stage ICR embryos. Following the confirmation of germ line transmission of the mutant allele,

the mice were backcrossed with the C57BL/6J background. Homozygous mice and their wild-type control littermates were obtained by heterozygous intercrossing. These mice are available on request from the RIKEN Bioresource Research Center (BRC; number BRC10613).

Rotarod performance test. The rotarod performance test was carried out using a rotarod apparatus (ENV-577M; Med Associates) with mice at 2 months of age. The rotation speed was 5 rpm at the beginning of the experiments and then gradually accelerated to 40 rpm. Parameters such as a pause in walking, grasping of the rod, and falling from the rod were recorded for a total of 240 s.

Plasmids. TUT1, SART3, LSm2, and LSm6 cDNAs were amplified from an HCT116 cell cDNA library by using KOD plus DNA polymerase (TOYOBO). TUT1 cDNA was inserted into pcDNA3-Flag, pCS4-Myc, and pCS4-EGFP vectors. SART3 cDNA was inserted into pCS4-Myc, pCS4-HA, and pCS4-EGFP vectors. LSm2 and LSm6 were inserted into the pCS4-Myc vector. SART3 deletion mutants were amplified from SART3 wild-type plasmids and constructed likewise. *Usp15* was amplified from the cDNA clone from the Kazusa DNA Research Institute and inserted into pcDNA3-Flag and pcDNA3-Myc vectors. The pCAGEN-His-Ub (wild-type and mutants) construct was described previously (57).

The primers used in this study were as follows: Lsm2 forward, 5′-AGGATCCGCCACCATGCTCTTCTAT TCTTTTTTCAAGTCCCTTG-3′, and reverse, 5′-GGGATCCTCACTGTTTCTGCTGCAGGGCTTCCTTCCTTGC-3′; Lsm6 forward, 5′-AGGATCCGCCACCATGAGTCTTCGGAAGCAAACCCCTAGTGACTTC-3′, and reverse, 5′-GG GATCCTCACATCCGTCTAAGATCTTCACTGTTTGCCCGCCTGTCTGCCAGGCTTCTTC-3′; SART3 forward, 5′-AA GATCTGCCACCATGGCGACTGCGGCCGAAAC-3′, and reverse, 5′-AAGATCTTCACTTTCTCAGAAACAGCTTGG CAAAATCG-3′; SART3$^{1-649}$ reverse, 5′-AAGATCTGTTCTCGACCCTTCTGCGTTTG-3′; SART3$^{278-649}$ forward, 5′-AAGATCTCCAGAGTCAGTAATTCAGAAC-3′; SART3$^{660-963}$ forward, 5′-AAGATCTGTAGAAGTAGCAGCAG GGCC-3′; TUT1 forward, 5′-AAGATCTGCCACCATGTCACTTCCTATCGGATCGGC-3′, and reverse, 5′-AAGAT CTTCACTTGAGATGTCGAATTGCTTG-3′.

Antibodies. For immunoblot analyses, anti-USP15 (Bethyl, A300-923A; Cell Signaling, D1K6S), anti-SART3 (Proteintech, 180251AP), antitubulin (Sigma, DM1A), anti-BiP (Cell Signaling, CB0B12), anti-TUT1 (Sigma, SAB4300788), anti-Flag (Sigma, M2), anti-Myc (Santa Cruz, 9E10), anti-green fluorescent protein (anti-GFP) (MBL, 598), and anti-His (GE Healthcare, 27-4710-01; MBL, PM032) IgGs were used as primary antibodies. The peroxidase-conjugated anti-mouse and anti-rabbit antibodies (SeraCare) were used as secondary antibodies. Anti-USP15 (Cell Signaling, D1K6S), anticalbindin (Sigma, CB-955), anti-cleaved caspase-3 (Cell Signaling, 5A1E), and anti-BiP (Cell Signaling, CB0B12) antibodies were used for immunohistochemical analyses as primary antibodies. For immunocytochemical analyses, anti-USP15 (Cell Signaling, D1K6S), anti-Flag (Sigma, M2; Sigma, F7425), and antihemagglutinin (anti-HA) (Roche, 3F10) antibodies were used as primary antibodies. Anti-NPM antibody was provided by Mitsuru Okuwaki (58). Alexa Fluor 488- and 594-conjugated anti-rabbit, anti-rat, and anti-mouse antibodies were used as secondary antibodies.

Cell culture and transfection. Wild-type and *Usp15*$^{-/-}$ mouse embryonic fibroblasts (MEFs), HEK293, HEK293T, and HeLa cells were cultured in Dulbecco's modified Eagle's medium (high glucose) (WAKO) supplemented with 10% fetal bovine serum and 1% penicillin-streptomycin-glutamine (Gibco) in a 37°C incubator with 5% CO_2. Cells were transfected using polyethyleneimine MAX (PEI Max) (Polysciences) for overexpression. The amount of the plasmids and PEI Max were optimized in proportion to the relative surface area and the number of cells. In the 60-mm dish, cells were plated 1.0×10^6 to 1.5×10^6 cells in 3 ml per dish and incubated at 5% CO_2 and 37°C for 1 day. The plasmids (4.0 to 12.0 μg) were mixed with 200 to 600 μl of Opti-MEM (Thermo Fisher), and 1.0 μg/μl of PEI Max (8.0 to 24.0 μl) was mixed with 200 to 600 μl of Opti-MEM in another tube. Both solutions were combined and incubated for 20 min at room temperature, followed by the adding of these mixtures to cells. Knockdowns of the target genes were utilized with Lipofectamine RNAi/MAX reagent (Life Technologies). The transfection procedure was according to the manufacturer's instructions. The control siRNA (MISSION siRNA universal negative control [SIC001]) was purchased from Sigma. The TUT1 siRNAs (MISSION siRNA; Merck) used in this study were as follows: TUT1 sense, 5′-GUCACAAUGUCGCAGCCAA-deoxyribosylthymine (dT)-3′, and antisense, 5′-UUGGCUGCGACAUUGUGACdTdT-3′; TUT1* sense, 5′-GUGGUCAAGUUCUGUCAUCdTdT-3′, and antisense, 5′-GAUGACAGAACUUGACCACdTdT-3′.

Histology. Organs collected from wild-type and *Usp15*$^{-/-}$ littermate mice were perfused with 4% paraformaldehyde in phosphate-buffered saline (4% PFA-PBS), fixed in the same fixative for overnight, and embedded in paraffin. Paraffin sections were then sliced into 2-μm sections and stained with Meyer's hematoxylin and eosin or subjected to immunohistochemical analyses.

Immunohistochemistry. The cerebellum of wild-type and *Usp15*$^{-/-}$ littermates at postnatal day 15 (P15) were perfused with 4% PFA-PBS and fixed with the same fixative for 3 h. After sucrose infiltration, the samples were embedded in OTC compound (Tissue-Tek) and sliced at a 30-μm thickness. Deparaffinized tissue specimens were immersed in 0.01 M citrate buffer (10 mM citric acid, 0.05% Tween 20, pH 6.0) and boiled in a microwave oven for 10 min. After antigen retrieval, tissue sections were blocked for 1 h in 3% bovine serum albumin (BSA) in TBST (25 mM Tris-HCl [pH 7.5], 0.14 M NaCl, 0.1% Triton X-100) and incubated with a primary antibody in TBST overnight at 4°C. Following the wash with TBST, tissue sections were incubated with a secondary antibody diluted 1/500 in TBST for 1 h at room temperature. Tissue specimens were observed using a fluorescence microscope (Keyence, BIOREVO BZ-9000) or a confocal laser scanning fluorescence microscope (Zeiss LSM700).

Immunoprecipitation and MS analysis. Cells were lysed with lysis buffer (20 mM Tris-HCl [pH 8.0], 150 mM NaCl, 1 mM EDTA, 0.5% NP-40, 1 mM dithiothreitol [DTT]) and centrifuged at 14,000 rpm for 10 min. The supernatant was immunoprecipitated with an anti-Myc antibody together with protein G-agarose beads (Thermo Scientific) or anti-Flag M2-agarose beads (Sigma) at 4°C for 3 h. The beads were then washed with lysis buffer and subjected to immunoblot analysis. The MS analysis has been described previously (59). Briefly,

overexpressed Flag-tagged USP15 in HEK293 cells was immunoprecipitated using an anti-Flag antibody and subjected to liquid chromatography-tandem mass spectrometry (LC-MS/MS) analysis.

His-ubiquitin pulldown assay. Cells were washed with PBS and lysed in extraction buffer (6 M guanidinium-HCl, 50 mM sodium phosphate buffer [pH 8.0], 300 mM NaCl, and 5 mM imidazole). Cell lysates were sonicated for 30 s on ice and incubated with Talon metal affinity resin (Clontech) at 4°C for 3 h. The precipitants were washed with buffer (50 mM sodium phosphate buffer [pH 8.0], 300 mM NaCl, and 5 mM imidazole) and subjected to immunoblot analysis.

Immunoblot analysis. Organs collected from wild-type and *Usp15*$^{-/-}$ mice were homogenized in lysis buffer (50 mM Tris-HCl [pH 8.0], 150 mM NaCl, 1 mM EDTA, 1% NP-40, 5% Na-deoxycholate, 0.1% SDS, 1 mM DTT) on ice and centrifuged at 14,000 rpm for 10 min. The supernatant was run on SDS-PAGE gels for protein separation, followed by electrophoretic transfer to a polyvinylidene difluoride membrane (Millipore). After 1 h of blocking at room temperature, membranes were incubated with primary antibodies overnight at 4°C. The proteins on the membrane were then detected with horseradish peroxidase (HRP)-conjugated secondary antibodies and chemiluminescence reagent (Amersham ECL Prime Western blotting detection reagents, GE Healthcare; Chemi-Lumi One Super, Nacalai Tesque). The immunoblotting data present the representative results from two or three independent experiments.

***In vitro* deubiquitination assay.** Recombinant ubiquitinated Myc-TUT1 was affinity purified from HEK293 cells expressing Myc-TUT1 and His-ubiquitin using Talon metal affinity resin. The precipitants were subjected to a deubiquitination reaction in the presence or absence of recombinant USP15 (LifeSensors) after the renaturation of recombinant proteins. The reaction mixture was incubated with DUB buffer (50 mM Tris-HCl [pH 7.5], 150 mM NaCl, 5 mM $MgCl_2$, and 10 mM DTT) at room temperature for 1 h. The samples were then analyzed by immunoblot analysis.

Immunocytochemistry. HeLa cells and MEFs were cultured on coverslips for 18 h and then transfected with the above-indicated plasmids. The cells were fixed with 4% paraformaldehyde in PBS for 10 min at room temperature. The cells on coverslips were blocked in 0.4% Triton X-100 in blocking solution (3% BSA in PBS) for 30 min at room temperature and then incubated with primary antibodies diluted in blocking solution for 1 h or overnight at 4°C. After washing with PBS, the cells were incubated with secondary antibodies (Alexa Fluor 488–anti-mouse IgG and Alexa Fluor 594–anti-rabbit IgG) diluted in blocking solution for 30 min at room temperature. Nuclei were stained with Hoechst 33342 (Life Technologies). The coverslips were then mounted onto slides using Fluoroshield mounting medium (ImmunoBioScience). Fluorescence images were obtained using a fluorescence microscope (Keyence model BZ-9000).

Measurement of polyadenylation activity. Flag-TUT1 was immunopurified from HEK293 cells with or without Myc-USP15 and subjected to a polyadenylation assay as described previously (60). Briefly, precipitated Flag-TUT1 was incubated with [α-^{32}P]ATP (29.6 TBq/mmol) and oligo(A)$_{12}$ RNA primer in reaction buffer [50 mM Tris-HCl (pH 8.3), 7% glycerol, 0.3% polyvinyl alcohol, 40 mM KCl, 0.5 mM $MnCl_2$, 25 mM $(NH_4)_2SO_4$, 0.25 mM DTT, 0.1 mM ATP, and RNase OUT (50 units)] at 30°C for the designated time. An aliquot of the reaction sample was spotted onto Whatman DE-81 paper, dried, and washed with 0.1 M phosphate buffer (pH 7.0) >8 times. Incorporation of AMP from [α-^{32}P]ATP into oligo(A)$_{12}$ RNA primer was measured using a liquid scintillation counter (Beckman LS 6500).

Quantitative real-time PCR. Total RNAs from wild-type and USP15-deficient cerebellum, cortex, and HEK293T cells were isolated by ISOGEN II (Nippon Gene) according to the manufacturer's instructions. The cDNAs were synthesized by reverse transcriptase and 100 units ReverTra Ace (TOYOBO) together with 25 pmol random hexamer primer (TOYOBO), 20 nmol deoxynucleoside triphosphates (dNTPs), and 0.5 to 5.0 μg total RNAs. The quantitative PCRs (qPCRs) were performed in triplicates in 96-well plates using Thunderbird SYBR qPCR mix (TOYOBO) and a Thermal Cycler Dice Real Time System TP800 (TaKaRa). The relative quantity of the target expression was calculated by comparative threshold cycle ($2^{-\Delta\Delta CT}$) methods using Thermal Cycler Dice Real Time System software (TaKaRa) with the following calculation: $\Delta\Delta C_T = (C_T^{\text{target}} - C_T^{5S})_{\text{sample}} - (C_T^{\text{target}} - C_T^{5S})_{\text{reference}}$. The following sequences were used as primers: 5S rRNA forward, 5′-CGGCCATACCACCCTGAAC-3′, and reverse, 5′-GCGGTCTCCCATCCAAGTA C-3′; U6-snRNA forward, 5′-GCTTCGGCAGCACATATACTAAAAT-3′, and reverse, 5′-ACGAATTTGCGTGTCATCC TT-3′; TUT1 forward, 5′-GATTCGGATGTCGAATCGCTG-3′, and reverse, 5′-CTGAGCAGAATCCACATCCCTG-3′; CHOP forward, 5′-ATATCTCATCCCCAGGAAACG-3′, and reverse, 5′-TCTTCCTTGCTCTTCCTCCTC-3′.

Exon array analysis. One-month-old wild-type and *Usp15*$^{-/-}$ mice ($n = 3$ per genotype) were euthanized using carbon dioxide. Their cerebellum and skeletal muscles were then dissected and frozen in liquid nitrogen. Total RNAs were extracted from each tissue using ISOGEN II (Nippon Gene) according to the manufacturer's instructions. The single-stranded cDNAs were generated from total RNA using an Ambion WT Expression kit (Ambion, Inc.), sequentially fragmented, and labeled using a GeneChip WT Terminal Labeling and Hybridization kit (Affymetrix). These samples were incubated at 45°C for 17 h to hybridize on Affymetrix GeneChip mouse exon 1.0 ST arrays. After hybridization, each probe array was washed and stained with Affymetrix GeneChip Fluidics Station 450 and scanned with an Affymetrix GeneChip Scanner 3000. Data were analyzed with GeneSpring 12.6 software and filtered by a splicing index of >0.5 and with a P value of <0.05.

The splicing index was calculated with the following calculation:

$$\text{splicing index} = \log_2\left(\text{NI}_{i1}/\text{NI}_{i2}\right)$$

$$\text{NI}_{ij} = E_{ij}/G_j$$

NI_{ij} means normalized intensity (NI) for exon i in experiment j. E_{ij} represents the estimated intensity level for exon i in experiment j. G_j is the estimated gene intensity.

Cytotoxicity assay. MEFs were plated on 96-well plates and incubated for 1 day. Cells were treated with thapsigargin and tunicamycin for 12 or 24 h and subjected to a cytotoxicity assay using a microplate reader model 680 (Bio-Rad) and Cell Counting Kit-8 (Dojindo) according to the manufacturer's instructions.

Statistical analysis. Statistical significance was analyzed by one-way analysis of variance (ANOVA) and Student's *t* test using Prism ver.6 software (GraphPad Software, Inc.).

Data availability. The GEO accession number for the array data set is GSE145385.

SUPPLEMENTAL MATERIAL

Supplemental material is available online only.

SUPPLEMENTAL FILE 1, XLSX file, 0.1 MB.

SUPPLEMENTAL FILE 2, XLSX file, 0.1 MB.

ACKNOWLEDGMENTS

We thank Toru Natsume (AIST, Japan) for helping with the proteomics experiments and all members of the laboratory for helpful discussions and technical support.

This work was supported by Grant-in-Aid from Ministry of Education, Science, Sports and Culture of Japan (JSPS KAKENHI 24111504, 23770218, 16KK0158), the Naito Foundation, and the Astellas Foundation for Research on Metabolic Disorders (FT).

REFERENCES

1. Black DL. 2003. Mechanisms of alternative pre-messenger RNA splicing. Annu Rev Biochem 72:291–336. https://doi.org/10.1146/annurev.biochem.72.121801.161720.
2. Li Q, Lee JA, Black DL. 2007. Neuronal regulation of alternative pre-mRNA splicing. Nat Rev Neurosci 8:819–831. https://doi.org/10.1038/nrn2237.
3. Vuong CK, Black DL, Zheng S. 2016. The neurogenetics of alternative splicing. Nat Rev Neurosci 17:265–281. https://doi.org/10.1038/nrn.2016.27.
4. Scotti MM, Swanson MS. 2016. RNA mis-splicing in disease. Nat Rev Genet 17:19–32. https://doi.org/10.1038/nrg.2015.3.
5. Wahl MC, Will CL, Luhrmann R. 2009. The spliceosome: design principles of a dynamic RNP machine. Cell 136:701–718. https://doi.org/10.1016/j.cell.2009.02.009.
6. Makarov EM, Makarova OV, Urlaub H, Gentzel M, Will CL, Wilm M, Luhrmann R. 2002. Small nuclear ribonucleoprotein remodeling during catalytic activation of the spliceosome. Science 298:2205–2208. https://doi.org/10.1126/science.1077783.
7. Rappsilber J, Ryder U, Lamond AI, Mann M. 2002. Large-scale proteomic analysis of the human spliceosome. Genome Res 12:1231–1245. https://doi.org/10.1101/gr.473902.
8. Bellare P, Small EC, Huang X, Wohlschlegel JA, Staley JP, Sontheimer EJ. 2008. A role for ubiquitin in the spliceosome assembly pathway. Nat Struct Mol Biol 15:444–451. https://doi.org/10.1038/nsmb.1401.
9. Song EJ, Werner SL, Neubauer J, Stegmeier F, Aspden J, Rio D, Harper JW, Elledge SJ, Kirschner MW, Rape M. 2010. The Prp19 complex and the Usp4Sart3 deubiquitinating enzyme control reversible ubiquitination at the spliceosome. Genes Dev 24:1434–1447. https://doi.org/10.1101/gad.1925010.
10. Das T, Park JK, Park J, Kim E, Rape M, Kim EE, Song EJ. 2017. USP15 regulates dynamic protein-protein interactions of the spliceosome through deubiquitination of PRP31. Nucleic Acids Res 45:5010–5011. https://doi.org/10.1093/nar/gkx062.
11. Sowa ME, Bennett EJ, Gygi SP, Harper JW. 2009. Defining the human deubiquitinating enzyme interaction landscape. Cell 138:389–403. https://doi.org/10.1016/j.cell.2009.04.042.
12. Cornelissen T, Haddad D, Wauters F, Van Humbeeck C, Mandemakers W, Koentjoro B, Sue C, Gevaert K, De Strooper B, Verstreken P, Vandenberghe W. 2014. The deubiquitinase USP15 antagonizes Parkin-mediated mitochondrial ubiquitination and mitophagy. Hum Mol Genet 23:5227–5242. https://doi.org/10.1093/hmg/ddu244.
13. Cornelissen T, Vilain S, Vints K, Gounko N, Verstreken P, Vandenberghe W. 2018. Deficiency of parkin and PINK1 impairs age-dependent mitophagy in *Drosophila*. Elife 7:e35878. https://doi.org/10.7554/eLife.35878.
14. Jongsma ML, Berlin I, Wijdeven RH, Janssen L, Janssen GM, Garstka MA, Janssen H, Mensink M, van Veelen PA, Spaapen RM, Neefjes J. 2016. An ER-associated pathway defines endosomal architecture for controlled cargo transport. Cell 166:152–166. https://doi.org/10.1016/j.cell.2016.05.078.
15. Eichhorn PJ, Rodon L, Gonzalez-Junca A, Dirac A, Gili M, Martinez-Saez E, Aura C, Barba I, Peg V, Prat A, Cuartas I, Jimenez J, Garcia-Dorado D, Sahuquillo J, Bernards R, Baselga J, Seoane J. 2012. USP15 stabilizes TGF-beta receptor I and promotes oncogenesis through the activation of TGF-beta signaling in glioblastoma. Nat Med 18:429–435. https://doi.org/10.1038/nm.2619.
16. Zou Q, Jin J, Hu H, Li HS, Romano S, Xiao Y, Nakaya M, Zhou X, Cheng X, Yang P, Lozano G, Zhu C, Watowich SS, Ullrich SE, Sun SC. 2014. USP15 stabilizes MDM2 to mediate cancer-cell survival and inhibit antitumor T cell responses. Nat Immunol 15:562–570. https://doi.org/10.1038/ni.2885.
17. Zou Q, Jin J, Xiao Y, Zhou X, Hu H, Cheng X, Kazimi N, Ullrich SE, Sun SC. 2015. T cell intrinsic USP15 deficiency promotes excessive IFN-gamma production and an immunosuppressive tumor microenvironment in MCA-induced fibrosarcoma. Cell Rep 13:2470–2479. https://doi.org/10.1016/j.celrep.2015.11.046.
18. Pauli EK, Chan YK, Davis ME, Gableske S, Wang MK, Feister KF, Gack MU. 2014. The ubiquitin-specific protease USP15 promotes RIG-I-mediated antiviral signaling by deubiquitylating TRIM25. Sci Signal 7:ra3. https://doi.org/10.1126/scisignal.2004577.
19. Zhang H, Wang D, Zhong H, Luo R, Shang M, Liu D, Chen H, Fang L, Xiao S. 2015. Ubiquitin-specific protease 15 negatively regulates virus-induced type I interferon signaling via catalytically-dependent and -independent mechanisms. Sci Rep 5:11220. https://doi.org/10.1038/srep11220.
20. Chiang C, Pauli EK, Biryukov J, Feister KF, Meng M, White EA, Munger K, Howley PM, Meyers C, Gack MU. 2017. The human papillomavirus E6 oncoprotein targets USP15 and TRIM25 to suppress RIG-I-mediated innate immune signaling. J Virol 92:e01737-17. https://doi.org/10.1128/JVI.01737-17.
21. Komander D, Reyes-Turcu F, Licchesi JD, Odenwaelder P, Wilkinson KD, Barford D. 2009. Molecular discrimination of structurally equivalent Lys 63-linked and linear polyubiquitin chains. EMBO Rep 10:466–473. https://doi.org/10.1038/embor.2009.55.
22. Zhang Q, Harding R, Hou F, Dong A, Walker JR, Bteich J, Tong Y. 2016. Structural basis of the recruitment of ubiquitin-specific protease USP15 by spliceosome recycling factor SART3. J Biol Chem 291:17283–17292. https://doi.org/10.1074/jbc.M116.740787.
23. Menzies FM, Huebener J, Renna M, Bonin M, Riess O, Rubinsztein DC. 2010. Autophagy induction reduces mutant ataxin-3 levels and toxicity in a mouse model of spinocerebellar ataxia type 3. Brain 133:93–104. https://doi.org/10.1093/brain/awp292.
24. Long L, Thelen JP, Furgason M, Haj-Yahya M, Brik A, Cheng D, Peng J, Yao T. 2014. The U4/U6 recycling factor SART3 has histone chaperone

activity and associates with USP15 to regulate H2B deubiquitination. J Biol Chem 289:8916–8930. https://doi.org/10.1074/jbc.M114.551754.
25. Park JK, Das T, Song EJ, Kim EE. 2016. Structural basis for recruiting and shuttling of the spliceosomal deubiquitinase USP4 by SART3. Nucleic Acids Res 44:5424–5437. https://doi.org/10.1093/nar/gkw218.
26. Trippe R, Guschina E, Hossbach M, Urlaub H, Luhrmann R, Benecke BJ. 2006. Identification, cloning, and functional analysis of the human U6 snRNA-specific terminal uridylyl transferase. RNA 12:1494–1504. https://doi.org/10.1261/rna.87706.
27. Kim J, Tsuruta F, Okajima T, Yano S, Sato B, Chiba T. 2017. KLHL7 promotes TUT1 ubiquitination associated with nucleolar integrity: implications for retinitis pigmentosa. Biochem Biophys Res Commun 494:220–226. https://doi.org/10.1016/j.bbrc.2017.10.049.
28. Yamashita S, Takagi Y, Nagaike T, Tomita K. 2017. Crystal structures of U6 snRNA-specific terminal uridylyltransferase. Nat Commun 8:15788. https://doi.org/10.1038/ncomms15788.
29. Hamilton G, Gillingwater TH. 2013. Spinal muscular atrophy: going beyond the motor neuron. Trends Mol Med 19:40–50. https://doi.org/10.1016/j.molmed.2012.11.002.
30. Lee EB, Lee VM, Trojanowski JQ. 2011. Gains or losses: molecular mechanisms of TDP43-mediated neurodegeneration. Nat Rev Neurosci 13:38–50. https://doi.org/10.1038/nrn3121.
31. Watson CN, Belli A, Di Pietro V. 2019. Small non-coding RNAs: new class of biomarkers and potential therapeutic targets in neurodegenerative disease. Front Genet 10:364. https://doi.org/10.3389/fgene.2019.00364.
32. Yahara M, Kitamura A, Kinjo M. 2017. U6 snRNA expression prevents toxicity in TDP-43-knockdown cells. PLoS One 12:e0187813. https://doi.org/10.1371/journal.pone.0187813.
33. Yamashita N, Mosinger B, Roy A, Miyazaki M, Ugajin K, Nakamura F, Sasaki Y, Yamaguchi K, Kolattukudy P, Goshima Y. 2011. CRMP5 (collapsin response mediator protein 5) regulates dendritic development and synaptic plasticity in the cerebellar Purkinje cells. J Neurosci 31:1773–1779. https://doi.org/10.1523/JNEUROSCI.5337-10.2011.
34. Norman DJ, Feng L, Cheng SS, Gubbay J, Chan E, Heintz N. 1995. The lurcher gene induces apoptotic death in cerebellar Purkinje cells. Development 121:1183–1193.
35. Lu Y, Qiu Y, Chen P, Chang H, Guo L, Zhang F, Ma L, Zhang C, Zheng X, Xiao J, Zhong R, Han L, Xu X, Zhang Y, Li D, Zhong G, Boyton R, Huang Y, He Y, Hu R, Wei B, Wang H. 2019. ER-localized Hrd1 ubiquitinates and inactivates Usp15 to promote TLR4-induced inflammation during bacterial infection. Nat Microbiol 4:2331–2346. https://doi.org/10.1038/s41564-019-0542-2.
36. Fukagai K, Waku T, Chowdhury A, Kubo K, Matsumoto M, Kato H, Natsume T, Tsuruta F, Chiba T, Taniguchi H, Kobayashi A. 2016. USP15 stabilizes the transcription factor Nrf1 in the nucleus, promoting the proteasome gene expression. Biochem Biophys Res Commun 478:363–370. https://doi.org/10.1016/j.bbrc.2016.07.045.
37. Naidoo N. 2009. ER and aging-protein folding and the ER stress response. Ageing Res Rev 8:150–159. https://doi.org/10.1016/j.arr.2009.03.001.
38. Lindholm D, Wootz H, Korhonen L. 2006. ER stress and neurodegenerative diseases. Cell Death Differ 13:385–392. https://doi.org/10.1038/sj.cdd.4401778.
39. Carew NT, Nelson AM, Liang Z, Smith SM, Milcarek C. 2018. Linking endoplasmic reticular stress and alternative splicing. Int J Mol Sci 19:3919. https://doi.org/10.3390/ijms19123919.
40. Janowicz A, Michalak M, Krebs J. 2011. Stress induced subcellular distribution of ALG-2, RBM22 and hSlu7. Biochim Biophys Acta 1813:1045–1049. https://doi.org/10.1016/j.bbamcr.2010.11.010.
41. Zhang C, Milunsky JM, Newton S, Ko J, Zhao G, Maher TA, Tager-Flusberg H, Bolliger MF, Carter AS, Boucard AA, Powell CM, Sudhof TC. 2009. A neuroligin-4 missense mutation associated with autism impairs neuroligin-4 folding and endoplasmic reticulum export. J Neurosci 29:10843–10854. https://doi.org/10.1523/JNEUROSCI.1248-09.2009.
42. Comoletti D, De Jaco A, Jennings LL, Flynn RE, Gaietta G, Tsigelny I, Ellisman MH, Taylor P. 2004. The Arg451Cys-neuroligin-3 mutation associated with autism reveals a defect in protein processing. J Neurosci 24:4889–4893. https://doi.org/10.1523/JNEUROSCI.0468-04.2004.
43. Wang J, Takeuchi T, Tanaka S, Kubo SK, Kayo T, Lu D, Takata K, Koizumi A, Izumi T. 1999. A mutation in the insulin 2 gene induces diabetes with severe pancreatic beta-cell dysfunction in the Mody mouse. J Clin Invest 103:27–37. https://doi.org/10.1172/JCI4431.
44. Fujita E, Dai H, Tanabe Y, Zhiling Y, Yamagata T, Miyakawa T, Tanokura M, Momoi MY, Momoi T. 2010. Autism spectrum disorder is related to endoplasmic reticulum stress induced by mutations in the synaptic cell adhesion molecule, CADM1. Cell Death Dis 1:e47. https://doi.org/10.1038/cddis.2010.23.
45. Dirnagl U, Simon RP, Hallenbeck JM. 2003. Ischemic tolerance and endogenous neuroprotection. Trends Neurosci 26:248–254. https://doi.org/10.1016/S0166-2236(03)00071-7.
46. Zhou L, Hang J, Zhou Y, Wan R, Lu G, Yin P, Yan C, Shi Y. 2014. Crystal structures of the Lsm complex bound to the 3′ end sequence of U6 small nuclear RNA. Nature 506:116–120. https://doi.org/10.1038/nature12803.
47. Inui M, Manfrin A, Mamidi A, Martello G, Morsut L, Soligo S, Enzo E, Moro S, Polo S, Dupont S, Cordenonsi M, Piccolo S. 2011. USP15 is a deubiquitylating enzyme for receptor-activated SMADs. Nat Cell Biol 13:1368–1375. https://doi.org/10.1038/ncb2346.
48. Jia Y, Mu JC, Ackerman SL. 2012. Mutation of a U2 snRNA gene causes global disruption of alternative splicing and neurodegeneration. Cell 148:296–308. https://doi.org/10.1016/j.cell.2011.11.057.
49. Bai B, Hales CM, Chen PC, Gozal Y, Dammer EB, Fritz JJ, Wang X, Xia Q, Duong DM, Street C, Cantero G, Cheng D, Jones DR, Wu Z, Li Y, Diner I, Heilman CJ, Rees HD, Wu H, Lin L, Szulwach KE, Gearing M, Mufson EJ, Bennett DA, Montine TJ, Seyfried NT, Wingo TS, Sun YE, Jin P, Hanfelt J, Willcock DM, Levey A, Lah JJ, Peng J. 2013. U1 small nuclear ribonucleoprotein complex and RNA splicing alterations in Alzheimer's disease. Proc Natl Acad Sci U S A 110:16562–16567. https://doi.org/10.1073/pnas.1310249110.
50. Lefebvre S, Burglen L, Reboullet S, Clermont O, Burlet P, Viollet L, Benichou B, Cruaud C, Millasseau P, Zeviani M. 1995. Identification and characterization of a spinal muscular atrophy-determining gene. Cell 80:155–165. https://doi.org/10.1016/0092-8674(95)90460-3.
51. Zhang Z, Lotti F, Dittmar K, Younis I, Wan L, Kasim M, Dreyfuss G. 2008. SMN deficiency causes tissue-specific perturbations in the repertoire of snRNAs and widespread defects in splicing. Cell 133:585–600. https://doi.org/10.1016/j.cell.2008.03.031.
52. Singh SK, Stogsdill JA, Pulimood NS, Dingsdale H, Kim YH, Pilaz LJ, Kim IH, Manhaes AC, Rodrigues WS, Jr, Pamukcu A, Enustun E, Ertuz Z, Scheiffele P, Soderling SH, Silver DL, Ji RR, Medina AE, Eroglu C. 2016. Astrocytes assemble thalamocortical synapses by bridging NRX1alpha and NL1 via Hevin. Cell 164:183–196. https://doi.org/10.1016/j.cell.2015.11.034.
53. Kobayashi A, Tsukide T, Miyasaka T, Morita T, Mizoroki T, Saito Y, Ihara Y, Takashima A, Noguchi N, Fukamizu A, Hirotsu Y, Ohtsuji M, Katsuoka F, Yamamoto M. 2011. Central nervous system-specific deletion of transcription factor Nrf1 causes progressive motor neuronal dysfunction. Genes Cells 16:692–703. https://doi.org/10.1111/j.1365-2443.2011.01522.x.
54. Wang W, Chan JY. 2006. Nrf1 is targeted to the endoplasmic reticulum membrane by an N-terminal transmembrane domain. Inhibition of nuclear translocation and transacting function. J Biol Chem 281:19676–19687. https://doi.org/10.1074/jbc.M602802200.
55. Das T, Kim EE, Song EJ. 2019. Phosphorylation of USP15 and USP4 regulates localization and spliceosomal deubiquitination. J Mol Biol 431:3900–3912. https://doi.org/10.1016/j.jmb.2019.07.023.
56. Kotani Y, Morito D, Sakata K, Ainuki S, Sugihara M, Hatta T, Iemura SI, Takashima S, Natsume T, Nagata K. 2017. Alternative exon skipping biases substrate preference of the deubiquitylase USP15 for mysterin/RNF213, the moyamoya disease susceptibility factor. Sci Rep 7:44293. https://doi.org/10.1038/srep44293.
57. Tsuruta F, Takebe A, Haratake K, Kanemori Y, Kim J, Endo T, Kigoshi Y, Fukuda T, Miyahara H, Ebina M, Baba T, Chiba T. 2016. SCFFbl12 increases p21Waf1/Cip1 expression level through atypical ubiquitin chain synthesis. Mol Cell Biol 36:2182–2194. https://doi.org/10.1128/MCB.00174-16.
58. Hisaoka M, Nagata K, Okuwaki M. 2014. Intrinsically disordered regions of nucleophosmin/B23 regulate its RNA binding activity through their inter- and intra-molecular association. Nucleic Acids Res 42:1180–1195. https://doi.org/10.1093/nar/gkt897.
59. Natsume T, Yamauchi Y, Nakayama H, Shinkawa T, Yanagida M, Takahashi N, Isobe T. 2002. A direct nanoflow liquid chromatography-tandem mass spectrometry system for interaction proteomics. Anal Chem 74:4725–4733. https://doi.org/10.1021/ac020018n.
60. Kashiwabara S, Zhuang T, Yamagata K, Noguchi J, Fukamizu A, Baba T. 2000. Identification of a novel isoform of poly(A) polymerase, TPAP, specifically present in the cytoplasm of spermatogenic cells. Dev Biol 228:106–115. https://doi.org/10.1006/dbio.2000.9894.